Controlled Etching of Internal and External Structures of SiO₂ Nanoparticles Using Hydrogen Bond of Polyelectrolytes

Md. Shahinul Islam,[†] Won San Choi,*[,‡] and Ha-Jin Lee*[,†]

[†]Western Seoul Center, Korea Basic Science Institute, 150 Bugahyun-ro, Seoudaemun-gu, Seoul, 120-140, Republic of Korea
[‡]Department of Chemical and Biological Engineering, Hanbat National University, 125 Dongseodaero, Yuseong-gu, Daejeon 305-719, Republic of Korea

S *Supporting Information*

ABSTRACT: We have demonstrated a novel strategy for the synthesis of mesoporous silica nanoparticles (MSNPs) using a surfactant-free method under ambient conditions. By the simple addition of an amine-based polymer (polyethylenimine; PEI) with a high molecular weight to a silica nanoparticle (SNP) solution, two types of MSNPs, including rambutan-like MSNPs (R-MSNPs) and hollow MSNPs (H-MSNPs), were produced. The structural changes of the MSNPs were systematically studied using various reaction conditions (reaction time, molar ratio and molecular weight of PEI, etc.) and were observed using electron microscopic techniques. The formation mechanisms of both MSNPs were carefully investigated using XPS, Raman, and IR spectroscopies. Because the synthesized MSNPs are highly porous materials that contain internal organic/inorganic networks, we investigated the removal/adsorption properties of these MSNPs with respect to pollutants toward possible future use in environmental remediation applications. The H-MSNPs exhibited better environmental remediation capabilities relative to the R-MSNPs because PEI is present between the cobweb-like internal structures of the H-MSNPs, thereby providing a significant number of reaction sites for the adsorption of pollutants. The approach presented here can also be used as a direct method for the preparation of intraconnected networks within the substructures.

KEYWORDS: *polyelectrolytes, mesoporous SiO₂, hydrogen bond, environmental remediation*
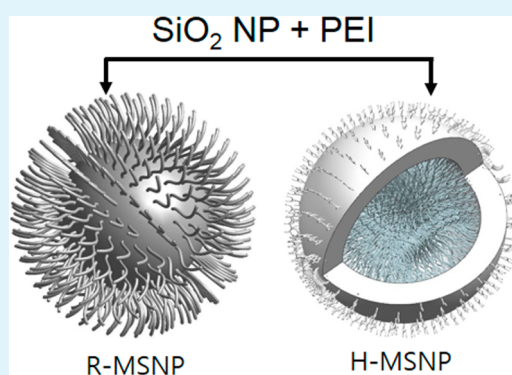
1. INTRODUCTION

Polyelectrolytes (PE) have been extensively investigated over the past decade because of their potential applications as micro/nanoreactors for chemical synthesis,[1−9] protective coatings against active materials,[10,11] containers exhibiting reversible permeability,[12−15] building blocks for nanoengineering,[16,17] and optical materials for antireflection coatings.[18,19] Most of these studies have focused on the PEs as templates or coating materials because the PEs provide an interesting platform for the exploitation of micro- and nanostructured materials with novel properties. Relatively little attention has been directed to reactions of the polyelectrolytes.

Mesoporous SiO₂ nanoparticles (MSNPs) are of continuous interest because of their unique properties, such as their high specific surface areas, controllable pore structures, and narrow pore size distributions.[20−23] MSNPs are typically synthesized by employing a surfactant-templated technique that induces the formation of porous silica structures by the spontaneous coassembly of the surfactants and inorganic precursors.[24−30] In this method, the surfactants in the solution play an important role in guiding the formation of porous inorganic structures from solubilized inorganic precursors. Thus, the presence of surfactants is thought to be critical for the formation of porous structures. However, surfactant removal is key for completing

the formation of MSNPs. The surfactants, which are often toxic substances, normally must be removed under harsh conditions, such as calcination (over 500 °C) or solvent extraction through refluxing in acidic alcohol for a minimum of 24 h.[31−36] A surfactant is necessary for the preparation of mesoporous structures; however, it can be difficult to avoid the cumbersome removal process that accompanies such surfactants. Therefore, there is significant interest in developing novel methods for the preparation of MSNPs without the use of surfactants, but relatively little attention has been focused on this area of research.

The modification of the interiors and exteriors of MSNPs with organic groups is of particular interest because of the possibility to combine a variety of functional groups with MSNPs. Two general methods, both of which involve co-condensation and postgrafting synthesis, have been used for the introduction of functional groups onto MSNPs. The former condensation method involves co-condensing hydrolyzed alkoxysilanes with inorganic precursors and results in a direct modification of the interior MSNP pores. The postgrafting

synthesis method involves modification after MSNP synthesis, which involves the reaction of alkoxysilanes with surface-accessible silanol groups in the interior and exterior of the MSNP.[37,38] However, both methods present several disadvantages. The co-condensation approach enables MSNPs to retain a homogeneous distribution of the functional groups at the expense of mesoscopic ordering. Thus, the functional groups embedded within the mesoporous network are restricted from further interaction with any materials that are subsequently added. Furthermore, the location and the loading amounts of the functional groups are not yet known.[39,40] Meanwhile, the postgrafting synthesis method typically results in inhomogeneous surface coverage because of the congregation of organic moieties near the mesopores and the exterior surfaces.[41] The low reactivity of the surface silanols also limits the extent of surface functionalization.[42] To summarize the process of MSNP synthesis, sacrificial surfactants should be used and removed when preparing mesoporous structures, and surface treatments should be performed either during or after the process to provide functionality of the mesoporous structures. The above-mentioned issues might be solvable if the existing process for MSNP synthesis can be simplified or omitted. This idea inspired us to explore a novel method for synthesizing MSNPs. In this work, we report an all-in-one approach for the synthesis of two types of MSNP at room temperature using polyelectrolytes; additionally, this approach does not include surfactant templating or surface modification (Scheme 1).

Scheme 1. Schematic Representation Showing Formation of the Rambutan-like Mesoporous SiO$_2$ NP (R-MSNP) and the Hollow Mesoporous SiO$_2$ NP (H-MSNP)
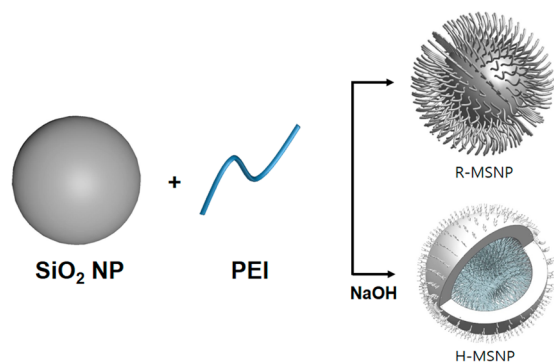
2. EXPERIMENTAL SECTION

Materials. Tetraethyl orthosilicate (TEOS, 99.99%), poly-(ethylenimine) (PEI, M_w = 750 kDa; 25 kDa and 2 kDa), lead(II) nitrate (Pb(NO$_3$)$_2$, 99.99%), chloroauric acid (HAuCl$_4$, 99.99%), mercury(II) nitrate (HgN$_2$O$_6$·H$_2$O, 98%), sodium arsenate (HAs-Na$_2$O$_4$, 98%), sodium borohydrate (NaBH$_4$), methyl orange, microcystin YR (M_w = 1045), ethyl alcohol, and ammonium hydroxide solution (28−30%) were purchased from Sigma-Aldrich. All chemicals were used without further purification. The PEI and metal precursor solutions were prepared with deionized (DI) water, obtained from a Millipore Simplicity 185 system.

Synthesis of the Rambutan-like MSNPs (R-MSNPs). The SNPs were prepared following a literature method, with few modifications: DI water (2 mL), ammonium hydroxide solution (0.2 mL), TEOS (0.8 mL), and ethanol (8 mL) were consecutively added to a glass vial while stirring, and milky white colored-SNPs developed following continued stirring for 6 h. To synthesize the R-MSNPs, an aqueous PEI solution (M_w = 750 kDa, 1 mg/mL) was added dropwise to the SNP solution while stirring until the desired mixed volume ratio for

Si/PEI (e.g., 1:1, 1:3, and 1:5) was obtained. Then, the SNP-PEI mixture was continuously stirred for 6 to 24 h at room temperature. Finally, the mixture was centrifuged, washed with ethanol to remove excess, and unbound PEI, and dried at room temperature. The synthesized Si/PEI was identified as rambutan-like MSNPs. For a comparison of the morphology change of the R-MSNPs, PEIs with different molecular weights (M_w = 25 kDa and 2 kDa) were also used instead of PEI of M_w = 750 kDa.

Synthesis of the Hollow MSNPs (H-MSNPs). An aqueous PEI solution was added dropwise to the SNP solution while stirring until the desired mixed volume ratio for Si/PEI (e.g., 1:1, 1:3, and 1:5) was obtained; the solution was then stirred for 30 min at room temperature. Afterward, 0.3 M aqueous NaOH solution was added dropwise to the SNP-PEI solution and stirred for 3 to 24 h. The final H-MSNPs were obtained by centrifugation, washing with ethanol several times, and drying the mixture at room temperature.

Characterization. The characterization of the fabricated MSNPs was carried out performing field-emission transmission electron microscopy (FE-TEM) on a JEOL JEM 2100F, and a Hitachi S-5500 was used for ultrahigh-resolution field-emission scanning electron microscopy (UHR-FESEM) analysis. The XPS studies were performed on an Axis NOVA (Kratos analytical) spectrometer operated with an aluminum anode (Al $K\alpha$, 1486.6 eV) at 600 W. The BET surface areas and BJH pore-size distributions were measured with an accelerated surface area and porosimetry system (Micromeritics ASAP2010, USA). The UV−vis absorption spectra were recorded on a UV−vis−NIR spectrophotometer (Shimadzu UV-3600). The MALDI-TOF MS analysis used here was performed in positive ion mode on a 4349 Voyager STR (Applied Biosystems) with an N$_2$ laser (337 nm), a repetition rate at 200 Hz, and an accelerating voltage of 20 kV. The heavy metal adsorption capacity was measured using a 7700s ICP-MS (Agilent Technologies).

3. RESULTS AND DISCUSSION

Panels a and b in Figure 1 present ultrahigh-resolution-scanning electron microscopy (UHR-SEM) images of SiO$_2$ NPs (SNPs) that were prepared in the absence of PEI and exhibit very smooth surfaces. However, at room temperature, the surfaces of the SNPs were gradually etched and projected only by the addition of PEI (Figure 1c). This phenomenon was observed for the high mixing ratio (Si/PEI = 1:5) of PEI, compared with its low mixing ratio (Si/PEI = 1:1) (Figure 1c$_1$−c$_3$). Similar results were observed when high-molecular-weight PEI (HMW-PEI) was used (M_w = 750 kDa), where fewer chains with short lengths were observed around the SNPs when using the low-molecular-weight PEI (M_w = 2 kDa) (LMW-PEI) (Figure 1d$_1$−d$_3$). The resulting SNPs were also produced by varying the reaction times (Figure 1e$_1$−e$_3$). The N$_2$ adsorption−desorption isotherm of the resulting NPs exhibited typical type-IV hysteresis, indicating a mesoporous structure (see Figure S1 in the Supporting Information). The Brunauer−Emmett−Teller (BET) specific surface area and Barrett−Joyner−Halenda (BJH) pore size were determined to be 97.2 m^2/g and 17.62 nm, respectively. The growth of the protruding chains formed using the above-mentioned parameters led to the formation of rambutan-like mesoporous SNPs (R-MSNP) (Figure 1f, g). To reveal the formation mechanism of the R-MSNPs, the reaction solution was collected and analyzed after the addition of PEI to the SNP solution. After the reaction had run to completion, the product solution contained R-MSNPs and short chain-like fragments. The energy-dispersive X-ray spectrometry (EDS) data revealed that the fragments were composed of Si and N, which originated from the SiO$_2$ and PEI, respectively (see Figure S2 in the Supporting Information). Thus, the SiO$_2$/PEI complex fragments were obtained from the etching of the SiO$_2$ surfaces as a result of the PEI
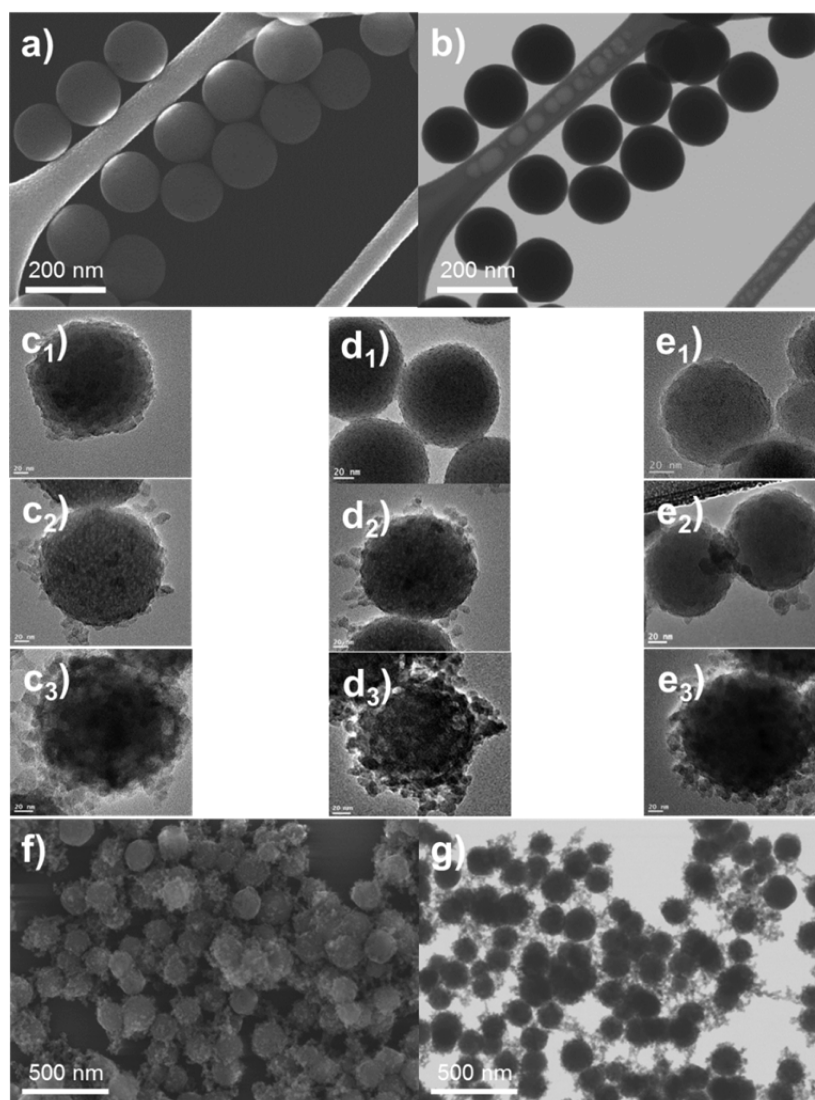
Figure 1. UHR-SEM and TEM images showing the formation process of R-MSNPs. UHR-SEM images of SNPs in (a) SE and (b) TE modes. TEM images of R-MSNPs prepared by (c) varying the PEI mixture volume ratio with a fixed volume of SNPs for (c_1) Si:PEI = 1:1, (c_2) Si:PEI = 1:3, and (c_3) Si:PEI = 1:5; by (d) varying the M_w of PEI as d_1) 2 kDa, (d_2) 25 kDa, and (d_3) 750 kDa; and by (e) varying the reaction time as (e_1) 6 h, (e_2) 12 h, and (e_3) 24 h. Also shown are (f) SE and (g) TE mode images of the R-MSNPs obtained from the optimized conditions. The asterisk denotes the main reaction conditions as a 1:5 mixing volume ratio of Si/PEI (M_w = 750 kDa) and a reaction time of 24 h under room temperature (i.e., Si:PEI$_{750\ kDa}$ = 1:5, 24 h, R.T.)*. Each parameter was changed based on the main reaction condition.

addition. Furthermore, images c and d in Figure 1 indicate that the R-MSNPs were predominantly formed with high fractions of HMW-PEI. All of these experiments used significant fractions of ethylenimine units. Branched HMW-PEI possesses primary, secondary, and tertiary amines within the structures.[43] This appears to be a favorable structure for network formation via H-bonding. The number of networks formed via H-bonding can be increased with the fraction of ethylenimine units. Thus, we assumed that the formation of R-MSNPs could be attributed to H-bond formation between PEI and SNPs, in addition to PEI and PEI.

Fourier-transform infrared spectroscopy (FT-IR), X-ray photoelectron spectroscopy (XPS), and Raman spectroscopy were performed to reveal the formation mechanism of the R-MSNPs. Si−O−Si (asymmetric), Si−OH, and Si−O stretching bands were observed at 1058, 886, and 785 cm^{-1}, respectively, for the bare SNPs (Figure 2a, curve i). However, the Si−OH and Si−O bands almost completely disappeared (i.e., the

intensity became very weak) after treatment with PEI (curve iii because the Si−OH groups reacted with the PEI to produce Si−O−Si linkages.[44] In curve iii for R-MSNP, the Si−O−Si peak was observed, whereas new −CH$_2$ groups were detected at 2920 (νC−H), 2825 (νC−H), and 1449 (δ C−H) cm^{-1}. Additionally, N−H stretching and bending vibrations were detected at 3374 (νN−H), 3290 (νN−H), 1632 (δN−H), and 1554 (δN−H) cm^{-1}, whereas these vibrations were not observed in the bare SNPs. These results suggest that the amino organic groups such as PEI were introduced onto the SNP surfaces.[45] It was difficult to observe more distinguishable peak (νN−H) at 3290 cm^{-1} for curve ii and iii because of the broad and strong absorption band above 3000 cm^{-1} influenced by −OH groups.[46] Among the various amine peaks, the intensity of the N−H peak detected at 1554 cm^{-1} was stronger in the MSNP compared with the PEI (curves iii and iv), which was attributed to the formation of H-bonding.[47]
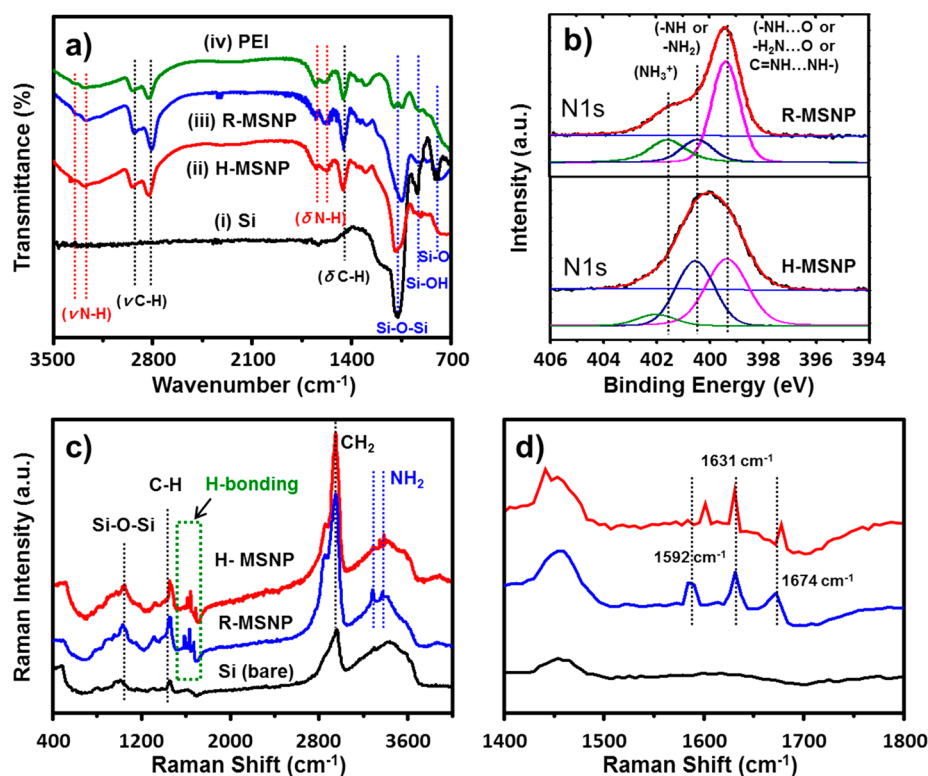
Figure 2. Comparison of the corresponding (a) FT-IR, (b) XPS, and (c, d) Raman spectroscopy analyses for R-MSNP and H-MSNP. R-MSNPs and H-MSNPs were prepared under reaction conditions of Si:PEI$_{750\ kDa}$ = 1:5 for 24 h at R.T. and Si:PEI$_{750\ kDa}$ = 1:5 with 0.3 M NaOH for 24 h at R.T., respectively.

The formation of H-bonds between the SNPs and PEI was further confirmed by XPS analysis. The shifting of the Si 2p peak (101.75−100.6 eV) indicates that interactions occurred between Si and PEI (see Figure S3 in the Supporting Information). The deconvoluted XPS spectrum of the N 1s peak contains a spectral line that is centered at 399.5 eV with an asymmetric tail extending toward higher binding energies (Figure 2b). The peaks correspond to the nitrogen atoms within the bonds of −H$_2$N···O and −NH···O (for SNP−PEI) or C=NH···HN− (for PEI−PEI).[44] These groups can readily form H-bonds and reside at lower ionization energies than free −NH− or −NH$_2$ groups (red line, <400 eV).[44] The presence of another weak peak at approximately 401.5 eV indicates that protonated amine groups (NH$_3^+$) are not involved in the formation of H-bonds (green line).[47,48] For R-MSNPs and H-MSNPs, the difference in binding energies of NH$_3^+$ results from the degree of asymmetry and broadening of the peak.[46] These results suggest that two types of H-bonds (SNP−PEI and PEI−PEI) can be formed in the R-MSNPs following PEI reaction with the SNPs. Because different types of intermolecular H-bonding can occur, Raman spectroscopy was used to confirm the degree (assay) of H-bonding of the Si-PEI. Si−O−Si vibrations were observed in the low frequency region (Figure 2c). The strong Raman bands detected in the region of 2800−3000 cm^{-1} were assigned as CH$_2$ stretching vibrations (navy line). The CH$_2$ peak detected in the base SNPs came from organic dust. The symmetric and asymmetric stretching bands of NH$_2$ were observed at 3349 and 3384 cm^{-1}, respectively; neither of these bands was observed in the bare SNPs (navy and black lines). After PEI treatment of the SNPs, several new peaks developed, indicating the formation of H-bonds with the bare SNPs (Figure 2c, d). The three peaks at 1592, 1629, and

1667 cm^{-1} were assigned to (i) the N−H bending vibration of H-bonds of the type SiO···H−NH, (ii) the NH$_2$ scissoring mode of H-bonds of the type SiO−H···NH$_2$, and (iii) the H-bonds of the free NH component (PEI) or water molecules, respectively.[49,50] These results further confirmed that two types of H-bonds, such as that between SNPs-PEI and PEI−PEI, are involved in the formation of the R-MSNPs. Compared to R-MSNPs, three peaks at 1602, 1631, and 1674 cm^{-1} with a blue shifting tendency were also assigned to the formation of H-bond as observed in the H-MNSPs (red line). For H-MSNPs, the surface morphology change caused by varying the pH conditions or H-bond by water molecules might be the reason for shifting of the Raman spectrum.[51] Furthermore, by considering the SiO$_2$ etching that occurs upon treatment with either HMW PEI or significant fractions of PEI, it appears that the formation of PEI networks via H-bonding affects the SiO$_2$ etching caused by interaction between PEI and SNPs. It is generally known that H-bonds are significantly weaker than covalent bonds. However, if HMW polymers form intermolecular networks with each other through H-bonding, the secondary interaction (H-bond) significantly increases in strength relative to the primary interaction (covalent bond).[52] In polymer science, depolymerization of the main chain can be accelerated if the side chains form a giant network based on H-bonding.[52] We suggest that the massive and heavy PEI networks, which are reinforced by a significant number of H-bonds, alter the balance of SiO$_2$ network conformation and promote the cleavage of primary covalent bonds (Si−O−Si). As a result, the PEI gradually etches the SiO$_2$ surface, leading to the formation of R-MSNPs. In support of this argument, the R-MSNPs formed predominantly when either a significant fraction of PEI or HMW-PEI was used, while no R-MSNPs
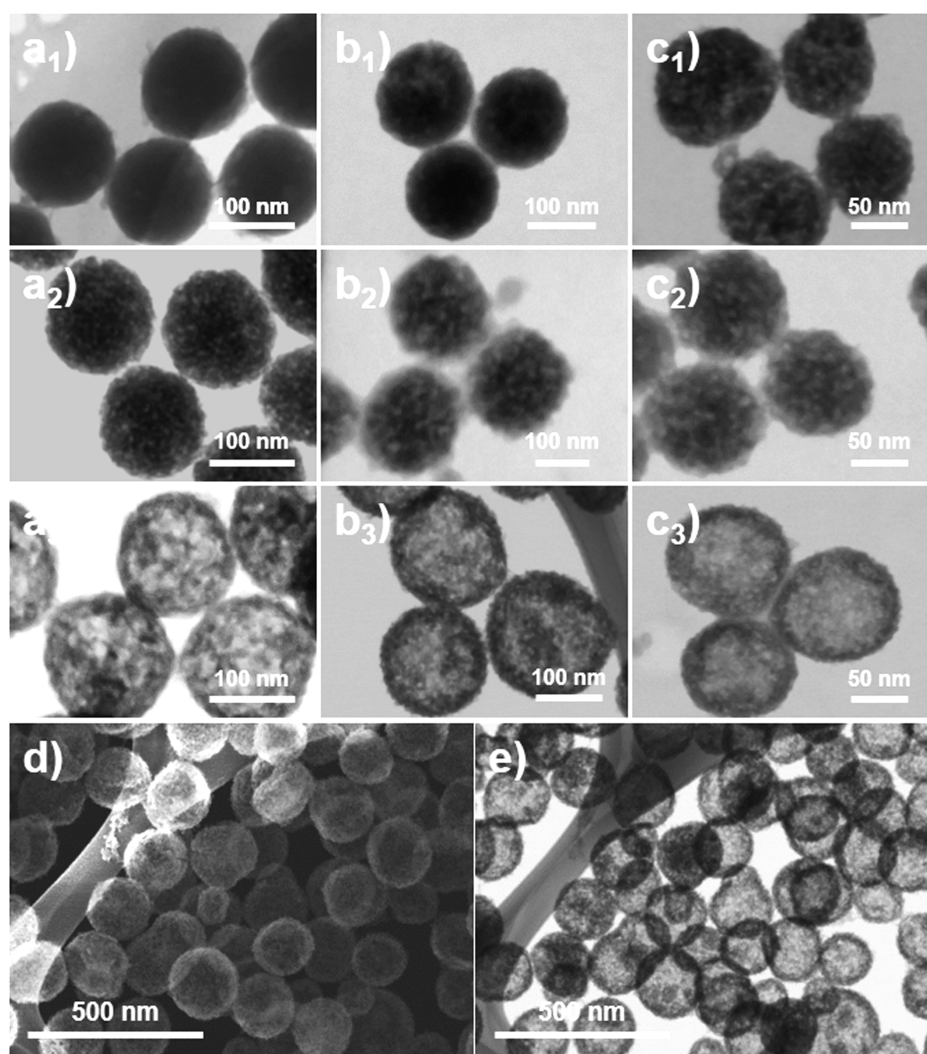
Figure 3. UHR-SEM and TEM images displaying the H-MSNP formation process. TEM images of H-MSNPs prepared by (a) varying the PEI mixing volume ratio with a fixed volume of SNPs as (a_1) Si:PEI = 1:1, (a_2) Si:PEI = 1:3, and (a_3) Si:PEI = 1:5; by (b) varying the M_w of PEI as (b_1) 2 kDa, (b_2) 25 kDa, and (b_3) 750 kDa; and by (c) varying the reaction time as (c_1) 6 h, (c_2) 12 h, and (c_3) 24 h. Also shown are (d) SE and (e) TE mode images of H-MSNPs obtained from the optimized conditions. The main reaction conditions for H-MSNPs were Si:PEI$_{750\ kDa}$ =1:5 with 0.3 M NaOH for 24 h at R.T. Each parameter was changed on the basis of the main reaction condition.

were formed in the case of a low fraction of PEI or LMW-PEI (Figure 1c, d).

To investigate the possibility of controlling MSNP morphology, the use of lower and higher pH conditions during R-MSNP fabrication (vs standard conditions at pH 8.1) was also investigated. By comparing the smooth surfaces of the bare SNPs, as shown in Figure 1a, b, hollow SNPs were produced after stirring the mixture (Si/PEI=1:5) in the presence of NaOH (0.3 M, pH 11) (Figures 3). All spheres with an average diameter of 125 nm exhibited pores oriented from the center to the outer surface. The N_2 adsorption−desorption isotherm shows that the hollow SNPs have a mesoporous structure (see Figure S4 in the Supporting Information). The BJH pore size and BET surface area were determined to be 37.56 nm and 53.62 m^2/g, respectively. Hollow MSNPs (H-MSNPs) were remarkably observed when a high mixing ratio of PEI (Si:PEI = 1:5), high molecular weight of PEI (M_w = 750 kDa), and prolonged reaction times, as shown in the R-MSNP cases (Figure 3a−c). FT-IR, XPS, and Raman analyses indicated that the formation of H-MSNPs is also related to H-bonding between the PEI and SiO$_2$ NPs, as well as between PEI and PEI

(Figure 2). Meanwhile, very interesting phenomena were observed within the H-MSNPs. To investigate thoroughly the internal structure of the H-MSNPs, we used electron tomography (ET); in ET, tomographic approaches are used to obtain detailed 3D models of substructure objects. A cobweb-like internal structure was observed within the H-MSNPs (Figure 4).

Although the density of the internal structure was not high compared to that of the shell structure, it appeared to connect each unit from end-to-end. Because these intraconnected networks consisted of PEI and SiO$_2$, as confirmed by FT-IR, XPS, and Raman spectroscopy (Figure 2), it was expected that intraconnected networks had formed within the H-MSNPs due to the etching of the SNPs following PEI penetration. This conclusion is further supported by the BET results, before and after H-MSNP calcination. As shown in the TEM image (Figures 3 and 4), it was expected that the H-MSNPs would show high surface areas due to the hollow and cobweb-like internal structures. However, the surface area was low (53.6 m^2/g). After calcination, the surface area of the H-MSNPs increased to 1025 m^2/g, which was approximately 20 times that
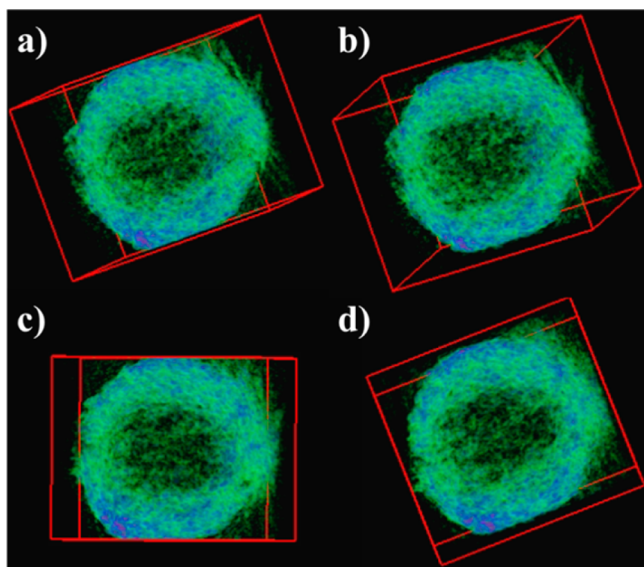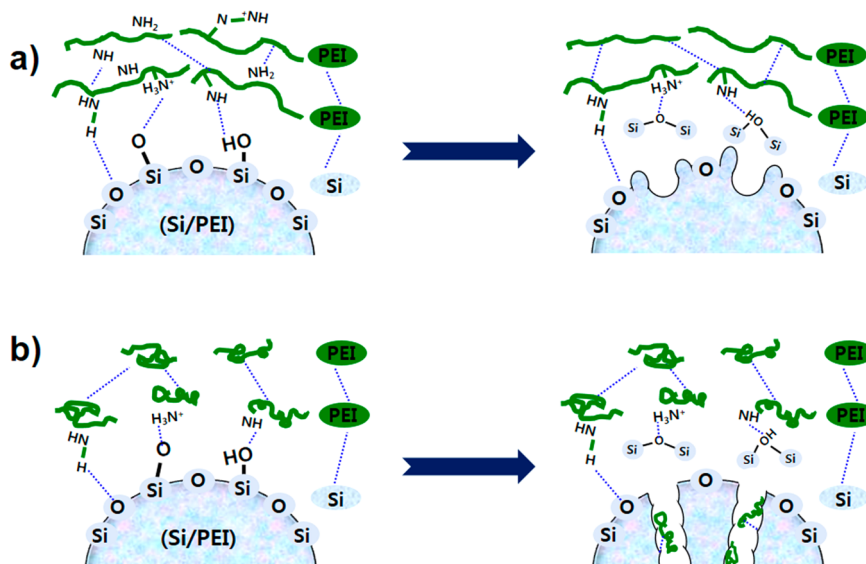
Figure 4. Electron tomography images of the H-MSNPs. (a−d) 3D images of the internal structure of the H-MSNPs obtained by varying the viewing angles.

of its original value before calcination (see Figure S5a in the Supporting Information). The structure of the H-MSNPs remained unchanged after calcination (see Figure S5b in the Supporting Information). This suggests that PEI is present in the spaces between the cobweb-like internal structures of the H-MSNPs. Thermogravimetric analysis (TGA) was carried out to determine the content of PEI within the H-MSNPs (see Figure S6 in the Supporting Information). Whether on or within the MSNPs, the PEI fraction should decompose thermally through two or three distinct steps. The total weight loss was approximately 20% for R-MSNPs with PEI on the surface; in contrast, approximately 34% was recorded for the H-MSNPs, which further supports our interpretation that a significant fraction of PEI exists within the cobweb-like internal structures of the H-MSNPs. It demonstrates that intra-connected networks were formed via SiO_2 etching by

interpenetration of PEI. Under low pH conditions, neither R- nor H-MSNPs were found, even after prolonged reaction times (see Figure S7 in the Supporting Information). At low pH values, the protonated fraction of PEI amine groups increased, whereas the surface charges of the SiO_2 decreased. A small amount of PEI adsorbed onto the SiO_2 surfaces due to increased polymer segment−segment repulsion and the presence of insufficient surface charges on the SiO_2.[43,50] As a result, the possibility of SiO_2 etching was low under low pH conditions.

To investigate further the formation mechanism of the H-MSNPs, the XPS fitting curve area, which displays the rate of H-bonding and the protonation of PEI, was considered (Figure 2b and S8). In the case of the H-MSNPs produced at pH = 11, 50.5% of the amine groups were involved in the formation of H-bonds, which is lower than the result for R-MSNP (61.5%) produced at pH 8 (see Figure S8 in the Supporting Information, curve 1). The contents of the protonated amine ($-NH_3^+$) were 17.5 and 7.2% for R- and H-MSNPs, respectively (see Figure S8 in the Supporting Information, curve 3). At pH 8, both the PEI and SNPs exhibit significant fractions of positive and negative charge states, respectively.[43] Therefore, the PEI loading on the SNP surface increased, and the PEI was able to etch the SNPs by taking advantage of the high rate of H-bonding (61.5%). Under these conditions, PEI favors a stretched form due to the presence of repulsion forces (protonated amines) within the chain (Scheme 2). Stretched PEIs mainly etched the SNP surfaces, but these PEI molecules were unable to penetrate into the SNP cores during the etching step due to the bulkiness of their stretched structures and the charge interactions between PEI and SiO_2. For this reason, surface-etched R-MSNPs were formed. However, at pH 11, PEI favored an entangled form due to the decreased fraction of protonated amine groups (17.5 to 7.2%) compared with PEI at pH 8 (see Figure S8 in the Supporting Information, curve 3). Branched PEI is neutral at pH $\geq$ 10.5.[43] Although the PEI loading on the SNP surfaces decreased, the PEI was still able to etch the SNPs as a result of the relatively high rate (50.5%) of H-bonding. Thus, the PEI was able to penetrate into the core of the SNPs while the PEI was able to etch the SNPs because of

Scheme 2. Schematic Representation of the Plausible Mechanism for the Formation of (a) the R-MSNPs and (b) the H-MSNPs

a)

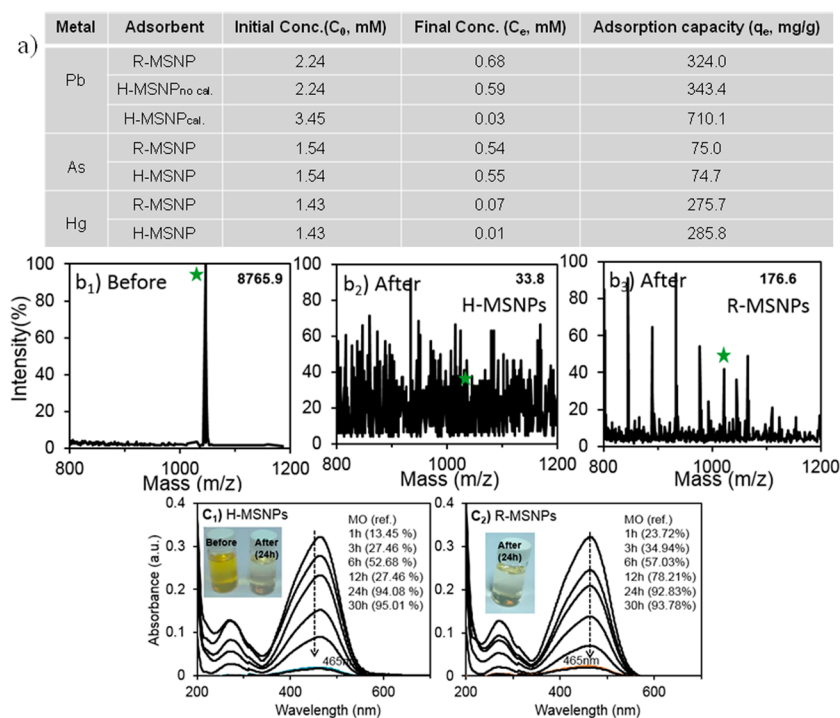| Metal	Adsorbent	Initial Conc.(C_0, mM)	Final Conc. (C_e, mM)	Adsorption capacity (q_e, mg/g)
Pb	R-MSNP	2.24	0.68	324.0
	H-MSNP$_{no\ cal.}$	2.24	0.59	343.4
	H-MSNP$_{cal.}$	3.45	0.03	710.1
As	R-MSNP	1.54	0.54	75.0
	H-MSNP	1.54	0.55	74.7
Hg	R-MSNP	1.43	0.07	275.7
	H-MSNP	1.43	0.01	285.8

Figure 5. (a) Summary of the maximum removal capacities of heavy metal ions by the R- and H-MSNPs. (b) MALDI-TOF mass spectra of the MC-YR solution (b_1) before and (b_2, b_3) after the treatment of R- and H-MSNPs, respectively. The peak for the $[MC\text{-}YR+H]^+$ ion is marked with an asterisk (*). The adsorption capacities of (c_1) H-MSNPs and (c_2) R-MSNPs for MO (methyl orange). The characteristic peak of MO at 465 nm decreased with increasing reaction time. All tests were performed in a dark room to avoid MO dye photodecomposition.

its entangled form and the decreased charge interactions between the PEI and SiO_2 (Scheme 2). Additionally, the entangled PEI nonuniformly etched the surface of the SNPs because the ratio of H-bonding of the H-MSNPs was lower than that of the R-MSNPs. Relatively large pores were formed as a result of the nonuniform etching process, as observed on the surfaces of the SNPs at the beginning of the reaction (see Figure S9 in the Supporting Information). As the reaction proceeded, the SNPs were gradually etched from their outside surfaces to the inside, while the PEI progressed into the center through the pore. For comparison, we tested SNPs at the same pH condition (pH 11) in the absence of PEI. Almost bare SNPs were observed, suggesting that the SiO_2 etching phenomena did not occur (see Figure S10 in the Supporting Information). NaOH seemed to play two roles in the case of the coexistence of NaOH with PEI. The NaOH increased the pH of the reaction medium, inducing a decrease in the rate of H-bonding of PEI and the entangled form of PEI. Thus, PEI was able to nonuniformly etch the SNPs from outside into the particle centered through the pores that formed initially. Furthermore, the reaction gradually progressed because the NaOH also helped the neutralized and entangled form of PEI to reach the SNP centers through the Si−O−Si network, which was swollen with hydroxyl ions.

The feasibility of the use of MSNPs as an environmental remediation material was explored. A test for the removal of heavy metal ions was performed using the MSNPs. Lead (Pb^{2+}), mercury (Hg^{2+}), and arsenate (AsO_4^{3-}) were used as the heavy metal ion sources. Figure 5a displays a summary of the heavy metal ion adsorption properties when the MSNPs were used as the adsorbent. The maximum removal capacities of the MSNPs were 343.3 mg/g for Pb, 285.8 mg/g for Hg, and 75.0 mg/g for As. These values are significantly higher than

those previously reported for similar systems.[53,54] Furthermore, calcinated H-MSNPs was also tested for the removal of heavy metal ions. As a representative one, result for the removal of Pb was 710.1 mg/g, which was doubly increased, compared to the H-MSNPs before calcination. It can be attributed to remarkable increase in the surface area (20 folds higher) of the H-MSNPs after calcination (see Figure S5 in the Supporting Information). This means that intranetwork SiO_2 structures possess a great active site to capture heavy metal ions even after elimination of PEI. For comparison, performance of bare SNPs was only 18.1 mg/g. A test for the removal of environmental contaminants, such as microcystins, was also performed using the MSNPs. Microcystins are potently hepatotoxic heptapeptides produced by cyanobacterial blooms in eutrophic water. Microcystin-YR (MC-YR) was used as the target adsorbate to evaluate the adsorption capability of the MSNPs. Figure 5b displays the MALDI-TOF mass spectra for the MC-YR before and after removal with the MSNPs. For comparison, the peak for the MC-YR is marked with an asterisk and is labeled with the intensity (S/N ratio). Before the MSNP treatment, the MC-YR intensity was very strong with an S/N ratio of 8,765. After the removal process, the MC-YR intensity decreased significantly, and the S/N ratios of 33.8 and 176.6 were barely detected for H-MSNPs and R-MSNPs, respectively. Calculations based on the S/N ratios for H- and R-MSNPs indicate that 99.7 and 98% of MC-YR were removed in the process. In another approach for environmental remediation, we also tested the MSNPs for the efficient disposal of wastewater containing organic toxic dyes, such as methyl orange (MO). The percentage of MO adsorption on the MSNPs increased with increasing exposure time in both cases. After the adsorption tests, the yellow color of the MO solution turns almost transparent. The H-MSNPs and R-MSNPs have high

adsorption rates (95 and 94%, respectively) for the MO dyes (Figure 5c). In most of the tests conducted here for the removal of environmental contaminants, the H-MSNPs performed better than the R-MSNPs due to the high loading of PEI within the hollow structure, as confirmed by the BET and TGA analyses (see Figures S5a and S6 in the Supporting Information). The above results indicate that PEI-containing MSNPs may be of potential use as environmental remediation materials.

4. CONCLUSIONS

We have demonstrated a novel strategy for the synthesis of MSNPs using a surfactant-free method at room temperature. By simply adding HMW-PEI to SNPs under different pH conditions, two types of MSNPs, including R-MSNPs and H-MSNPs, were produced. During the reaction, PEI forms H-bond networks between PEI and PEI, as well as between the PEI and SNPs. Massive and heavy PEI networks, reinforced by a significant number of H-bonds, alter the balance of the SiO_2 network conformation and promote the cleavage of primary covalent bond (Si−O−Si). The degrees of H-bonding and PEI protonation can be controlled by pH. With significant amounts of H-bonding and PEI protonation, PEI favors its stretched form due to the repulsion force between protonated amines within the chain. The stretched PEIs mainly etched the surface of SNPs via H-bonding, but they were unable to penetrate into the core of the SNPs during the etching process due to the bulkiness of their structures and the charge interaction between PEI and SiO_2. Consequently, the PEI gradually etched the SiO_2 surface and formed the R-MSNPs. With low amounts of H-bonding and PEI protonation, PEI favors its neutralized entangled form because of the reduced fraction of protonated amines. Thus, the PEI was able to penetrate into the SNP cores while the entangled PEI randomly or nonuniformly etched the SNPs due to decreased H-bonding and charge interaction. Finally, the PEI induced the development of H-MSNPs with a cobweb-like internal structure. The MSNPs exhibited excellent environmental remediation abilities for the removal/adsorption of pollutants. Overall, the H-MSNPs exhibited better environmental remediation abilities compared with the R-MSNPs because PEI was present between all of the cobweb-like internal structures of the H-MSNPs, thereby providing a significant number of reaction sites for the adsorption of pollutants. This approach can also be used as a direct method for the preparation of intraconnected networks within such sub-structures. We believe that this novel approach will be useful for the controlled-structure synthesis of various types of mesoporous inorganics.

■ ASSOCIATED CONTENT

ⓢ Supporting Information

Figures S1−S10. This material is available free of charge via the Internet at http://pubs.acs.org.

■ AUTHOR INFORMATION

Corresponding Authors
*E-mail: choiws@hanbat.ac.kr.
*E-mail: hajinlee@kbsi.re.kr.

Notes
The authors declare no competing financial interest.

■ REFERENCES

(1) Shchukin, D. G.; Sukhorukov, G. B.; Möhwald, H. Smart Inorganic/Organic Nanocomposite Hollow Microcapsules. *Angew. Chem., Int. Ed.* **2003**, *42*, 4472−4475.

(2) Choi, W. S.; Park, J.-H.; Koo, H. Y.; Kim, J.-Y.; Cho, B. K.; Kim, D.-Y. Grafting-From" Polymerization Inside a Polyelectrolyte Hollow-Capsule Microreactor. *Angew. Chem., Int. Ed.* **2005**, *44*, 1096−1101.

(3) Kidambi, S.; Dai, J.; Li, J.; Bruening, M. L. Selective Hydrogenation by Pd Nanoparticles Embedded in Polyelectrolyte Multilayers. *J. Am. Chem. Soc.* **2004**, *126*, 2658−2659.

(4) Lee, D.; Rubner, M. F.; Cohen, R. E. Formation of Nanoparticle-Loaded Microcapsules Based on Hydrogen-Bonded Multilayers. *Chem. Mater.* **2005**, *17*, 1099−1105.

(5) Radtchenko, I. L.; Giersig, M.; Sukhorukov, G. B. Inorganic Particle Synthesis in Confined Micron-Sized Polyelectrolyte Capsules. *Langmuir* **2002**, *18*, 8204−8208.

(6) Shchukin, D. G.; Sukhorukov, G. B. Nanoparticle Synthesis in Engineered Organic Nanoscale Reactors. *Adv. Mater.* **2004**, *16*, 671−682.

(7) Choi, W. S.; Koo, H. Y.; Park, J.-H.; Kim, D.-Y. Synthesis of Two Types of Nanoparticles in Polyelectrolyte Capsule Nanoreactors and Their Dual Functionality. *J. Am. Chem. Soc.* **2005**, *127*, 16136−16142.

(8) Peyratout, C. S.; Dähne, L. Tailor-Made Polyelectrolyte Microcapsules: From Multilayers to Smart Containers. *Angew. Chem., Int. Ed.* **2004**, *43*, 3762−3783.

(9) Dähne, L.; Leporatti, S.; Donath, E.; Möhwald, H. Fabrication of Micro Reaction Cages with Tailored Properties. *J. Am. Chem. Soc.* **2001**, *123*, 5431−5436.

(10) Shchukin, D. G.; Shutava, T.; Shchukina, E.; Sukhorukov, G. B.; Lvov, Y. M. Modified Polyelectrolyte Microcapsules as Smart Defense Systems. *Chem. Mater.* **2004**, *16*, 3446−3451.

(11) Shchukin, D. G.; Zheludkevich, M.; Yasakau, K.; Lamaka, S.; Ferreira, M. G. S.; Möhwald, H. Layer-by-Layer Assembled Nano-containers for Self-Healing Corrosion Protection. *Adv. Mater.* **2006**, *18*, 1672−1678.

(12) Dejugnat, C.; Halozan, D.; Sukhorukov, G. B. Defined Picogram Dose Inclusion and Release of Macromolecules Using Polyelectrolyte Microcapsules. *Macromol. Rapid Commun.* **2005**, *26*, 961−967.

(13) Shchukin, D. G.; Köhler, K.; Möhwald, H. Microcontainers with Electrochemically Reversible Permeability. *J. Am. Chem. Soc.* **2006**, *128*, 4560−4561.

(14) Ibarz, G.; Dähne, L.; Donath, E.; Möhwald, H. Smart Micro- and Nanocontainers for Storage, Transport, and Release. *Adv. Mater.* **2001**, *13*, 1324−1327.

(15) Sukhorukov, G. B.; Antipov, A. A.; Voigt, A.; Donath, E.; Möhwald, H. pH-Controlled Macromolecule Encapsulation in and Release from Polyelectrolyte Multilayer Nanocapsules. *Macromol. Rapid Commun.* **2001**, *22*, 44−46.

(16) Caruso, F.; Caruso, R. A.; Möhwald, H. Nanoengineering of Inorganic and Hybrid Hollow Spheres by Colloidal Templating. *Science* **1998**, *282*, 1111−1114.

(17) Caruso, F. Nanoengineering of Particle Surfaces. *Adv. Mater.* **2001**, *13*, 11−22.

(18) Hiller, J.; Mendelsohn, J. D.; Rubner, M. F. Reversibly Erasable Nanoporous Anti-Reflection Coatings from Polyelectrolyte Multi-layers. *Nat. Mater.* **2002**, *1*, 59−63.

(19) Koo, H. Y.; Yi, D. K.; Yoo, S. J.; Kim, D.-Y. A Snowman-like Array of Colloidal Dimers for Antireflecting Surfaces. *Adv. Mater.* **2004**, *16*, 274−277.

(20) Kresge, C. T.; Leonowicz, M. E.; Roth, W. J.; Vartuli, J. C.; Beck, J. S. Ordered Mesoporous Molecular Sieves Synthesized by a Liquid-Crystal Template Mechanism. *Nature* **1992**, *359*, 710−712.

(21) Ying, J. Y.; Mehnert, C. P.; Wong, M. S. Synthesis and Applications of Supramolecular-Templated Mesoporous Materials. *Angew. Chem., Int. Ed.* **1999**, *38*, 56−77.

(22) Brinker, C. J. Porous Inorganic Materials. *Curr. Opin. Solid State Mater. Sci.* **1996**, *1*, 798−805.

(23) Raman, N. K.; Anderson, M. T.; Brinker, C. J. Template-Based Approaches to the Preparation of Amorphous, Nanoporous Silicas. *Chem. Mater.* **1996**, *8*, 1682−1701.

(24) Polshettiwar, V.; Cha, D.; Zhang, X.; Basset, J. M. High-Surface-Area Silica Nanospheres (KCC-1) with a Fibrous Morphology. *Angew. Chem., Int. Ed.* **2010**, *49*, 9652−9656.

(25) Wu, J.; Zhu, Y. J.; Cao, S. W.; Chen, F. Hierachically Nanostructured Mesoporous Spheres of Calcium Silicate Hydrate: Surfactant-Free Sonochemical Synthesis and Drug-Delivery System with Ultrahigh Drug-Loading Capacity. *Adv. Mater.* **2010**, *22*, 749−753.

(26) Ji, Q.; Acharya, S.; Hill, P. J.; Vinu, A.; Yoon, S. B.; Yu, J.; Sakamoto, K.; Ariga, K. Hierarchic Nanostructure for Auto-Modulation of Material Release: Mesoporous Nanocompartment Films. *Adv. Funct. Mater.* **2009**, *19*, 1792−1799.

(27) Shiomi, T.; Tsunoda, T.; Kawai, A.; Matsuura, S.-I.; Mizukami, F.; Sakaguchi, K. Synthesis of a Cagelike Hollow Aluminosilicate with Vermiculate Micro-through-Holes and its Application to Ship-in-Bottle Encapsulation of Protein. *Small* **2009**, *5*, 67−71.

(28) Kassab, H.; Maksoud, M.; Aguado, S.; Pera-Titus, M.; Albela, B.; Bonneviot, L. Polyethylenimine Covalently Grafted on Mesostructured Porous Silica for CO₂ Capture. *RSC Adv.* **2012**, *2*, 2508−2516.

(29) Liong, M.; Lu, J.; Kovochich, M.; Xia, T.; Ruehm, S. G.; Nel, A. E.; Tamanoi, F.; Zink, J. I. Multifunctional Inorganic Nanoparticles for Imaging, Targeting, and Drug Delivery. *ACS Nano* **2008**, *2*, 889−896.

(30) Yi, D. K.; Lee, S. S.; Papaefthymiou, G. C.; Ying, J. Y. Nanoparticle Architectures Templated by SiO_2/Fe_2O_3 Nanocomposites. *Chem. Mater.* **2006**, *18*, 614−619.

(31) Rosenholm, J. M.; Meinander, A.; Peuhu, E.; Niemi, R.; Eriksson, J. E.; Sahlgren, C.; Linden, M. Targeting of Porous Hybrid Silica Nanoparticles to Cancer Cells. *ACS Nano* **2009**, *3*, 197−206.

(32) Tarn, D.; Ashley, C. E.; Xue, M.; Carnes, E. C.; Zink, J. I.; Brinker, A. J. Mesoporous Silica Nanoparticle Nanocarriers: Biofunctionality and Biocompatibility. *Acc. Chem. Res.* **2013**, *46*, 792−801.

(33) Shiju, N. R.; Alberts, A. H.; Khalid, S.; Brown, D. R.; Rothenberg, G. Mesoporous Silica with Site-Isolated Amine and Phosphotungstic Acid Groups: A Solid Catalyst with Tunable Antagonistic Functions for One-Pot Tandem Reactions. *Angew. Chem., Int. Ed.* **2011**, *50*, 9615−9619.

(34) Schuster, J.; He, G.; Mandlmeier, B.; Yim, T.; Lee, K. T.; Bein, T.; Nazar, L. F. Spherical Ordered Mesoporous Carbon Nanoparticles with High Porosity for Lithium−Sulfur Batteries. *Angew. Chem., Int. Ed.* **2012**, *51*, 3591−3595.

(35) Qiao, Z.-A.; Guo, B.; Binder, A. J.; Chen, J.; Veith, G. M.; Dai, S. Controlled Synthesis of Mesoporous Carbon Nanostructures via a "Silica-Assisted" Strategy. *Nano Lett.* **2013**, *13*, 207−212.

(36) Du, X.; He, J. Hierarchically Mesoporous Silica Nanoparticles: Extraction, Amino-Functionalization, and Their Multipurpose Potentials. *Langmuir* **2011**, *27*, 2972−2979.

(37) Meng, H.; Xue, M.; Xia, T.; Ji, Z.; Tarn, D. Y.; Zink, J. I.; Nel, A. E. Use of Size and a Copolymer Design Feature To Improve the Biodistribution and the Enhanced Permeability and Retention Effect of Doxorubicin-Loaded Mesoporous Silica Nanoparticles in a Murine Xenograft Tumor Model. *ACS Nano* **2011**, *5*, 4131−4144.

(38) Feng, X.; Fryxell, G. E.; Wang, L. Q.; Kim, A. Y.; Liu, J.; Kemner, K. M. Functionalized Monolayers on Ordered Mesoporous Supports. *Science* **1997**, *276*, 923−926.

(39) Walcarius, A.; Delacote, C. Rate of Access to the Binding Sites in Organically Modified Silicates. 3. Effect of Structure and Density of Functional Groups in Mesoporous Solids Obtained by the Co-Condensation Route. *Chem. Mater.* **2003**, *15*, 4181−4192.

(40) Richer, R. Direct Synthesis of Functionalized Mesoporous Silica by Non-Ionic Alkylpolyethyleneoxide Surfactant Assembly. *Chem. Commun.* **1998**, 1775−1777.

(41) Lim, M. H.; Stein, A. Comparative Studies of Grafting and Direct Syntheses of Inorganic−Organic Hybrid Mesoporous Materials. *Chem. Mater.* **1999**, *11*, 3285−3295.

(42) Kim, O. K.; Cho, S. J.; Park, J. W. Hyperbranching Polymerization of Aziridine on Silica Solid Substrates Leading to a Surface of Highly Dense Reactive Amine Groups. *J. Colloid Interface Sci.* **2003**, *260*, 374−378.

(43) Meszaros, R.; Thompson, L.; Bos, M.; Groot, P. D. Adsorption and Electrokinetic Properties of Polyethylenimine on Silica Surfaces. *Langmuir* **2002**, *18*, 6164−6169.

(44) Balas, F.; Manzano, M.; Horicajada, P.; Vallet-regi, M. Confinement and Controlled Release of Bisphosphonates on Ordered Mesoporous Silica-Based Materials. *J. Am. Chem. Soc.* **2006**, *128*, 8116−8117.

(45) Piers, A. S.; Rochester, C. H. Infrared Study of the Adsorption of 1-Aminopropyltrialkoxysilanes on Silica at the Solid/Liquid Interface. *J. Colloid Interface Sci.* **1995**, *174*, 97−103.

(46) Maäkilä, E.; Bimbo, L.; Kaasalainen, M.; Herranz, B.; Airaksinen, A. J.; Heinonen, M.; Kukk, E.; Hirvonen, J.; Santos, H. A.; Salonen, J. Amine Modification of Thermally Carbonized Porous Silicon with Silane Coupling Chemistry. *Langmuir* **2012**, *28*, 14045−14054.

(47) Patwardhan, S. V.; Emami, F. S.; Berry, R. J.; Jones, S. E.; Naik, R. R.; Deschaume, O.; Heinz, H.; Perry, C. C. Chemistry of Aqueous Silica Nanoparticle Surfaces and the Mechanism of Selective Peptide Adsorption. *J. Am. Chem. Soc.* **2012**, *134*, 6244−6256.

(48) Li, W.; Xu, Y.; Zhou, Y.; Ma, W.; Wang, S.; Dai, Y. Silica Nanoparticles Functionalized via Click Chemistry and ATRP for Enrichment of Pb(II) Ion. *Nanoscale Res. Lett.* **2012**, *7*, 485.

(49) Volovšček, V.; Furić, K.; Bistričić, L.; Lekovac, M. Micro Raman Spectroscopy of Silica Nanoparticles Treated with Aminopropylsilane-triol. *Macromol. Symp.* **2008**, *265*, 178−182.

(50) McKittrick, M. W.; Jones, C. W. Toward Single-Site Functional MaterialsPreparation of Amine-Functionalized Surfaces Exhibiting Site-Isolated Behavior. *Chem. Mater.* **2003**, *15*, 1132−1139.

(51) Max, J.-J.; Chapados, C. Isotope Effects in Liquid Water by Infrared Spectroscopy. III. H_2O and D_2O Spectra from 6000 to 0 $cm^{−1}$. *J. Chem. Phys.* **2009**, *131*, 184505.

(52) Deanin, R. D. Polymer Structure, Properties and Applications *Cahners Books* **1972**, Boston.

(53) Hu, J.-S.; Zhong, L.-S.; Song, W.-G.; Wan, L.-J. Synthesis of Hierarchically Structured Metal Oxides and their Application in Heavy Metal Ion Removal. *Adv. Mater.* **2008**, *20*, 2977−2982.

(54) Zhong, L.-S.; Hu, J.-S.; Liang, H.-P.; Cao, A.-M.; Song, W.-G.; Wan, L.-J. Self-Assembled 3D Flowerlike Iron Oxide Nanostructures and Their Application in Water Treatment. *Adv. Mater.* **2006**, *18*, 2426−2431.